

Development of the Reference Model for a Residential Heat Pump System for Cooling Mode Fault Detection and Diagnosis

Minsung Kim⁽¹⁾, Seok Ho Yoon⁽²⁾, W. Vance Payne^{(3)*} and Piotr A. Domanski⁽³⁾

⁽¹⁾Geothermal Energy Research Center, Korea Institute of Energy Research, Daejeon 305-343, Korea

⁽²⁾Energy Systems Research Division, Korea Institute of Machinery and Materials, Daejeon 305-343, Korea

⁽³⁾HVAC&R Equipment Performance Group, National Institute of Standards and Technology, Gaithersburg, MD 20899-8631, USA

Abstract

Development of a reference model to predict the value of system parameters during fault-free operation is a basic step for fault detection and diagnosis (FDD). In order to develop an accurate and effective reference model of a heat pump system, experimental data that cover a wide range of operating conditions are required. In this study, laboratory data were collected under various operating conditions and then filtered through a moving window steady-state detector. Over five thousand scans of steady-state data were used to develop polynomial regression models of seven system features. A reference model was also developed using an artificial neural network (ANN), and it is compared to the polynomial models.

Keywords: air conditioner, artificial neural network, fault detection and diagnosis, heat pump, polynomial reference model

Official contribution of the National Institute of Standards and Technology; not subject to copyright

* Corresponding author. Tel: +1-301-975-6663; fax: +1-301-975-8973.

E-mail address: vance.payne@nist.gov

Nomenclature

a	coefficient of multivariate polynomial
ANN	Artificial neural network
c	offset used in the sigmoid function
COP	coefficient of performance
CMF	compressor or reversing valve fault
DB	dry bulb
F	<i>feature</i>
FDD	fault detection and diagnosis
g	number of coefficients minus one in a reduced model
$h1, h2, h3$	ANN hidden layer neurons
$i1, i2, i3$	ANN input layer neurons
LL	refrigerant liquid line
m	number of coefficient in the regression model
MFR	mass flow rate
MPR	multivariate polynomial regression
MSR	mean squared residual
N	number of data samples used to generate the regression model
o	ANN output layer neurons
P	pressure
s	variable used within the sigmoid function of Equation 2
SSR	sum of squared residuals
T	temperature (°C)
w	hidden node weighting factor in Equation 2 for the k^{th} input
x	input to hidden node of the ANN model

Greek symbols

Δ	difference
$\phi^{(n)}$	feature or performance parameter of n^{th} order model

Subscripts

C	condenser
CA	condenser air
D	compressor discharge
drop	comparison of two identical models where one model has had some terms removed
E	evaporator
EA	evaporator air
full	refers to the model with a complete number of coefficients
i	feature index
ID	indoor
IDP	indoor dew point
k	number of data samples in a moving window or input number in Equation 2
meas	measured
n	time index for moving window method
OD	outdoor
pred	predicted
reduced	refers to a model with some of the coefficients removed
sat	saturation
sc	subcooling
sh	superheat

1. Introduction

A survey of over 55000 air conditioning units in the United States showed that more than 90 % were operating with one or more kinds of faults (Proctor, 2004). In another study, the average operating efficiency of the 1468 roof top units surveyed was 80 % of designed performance with 63 % of these units having performance degradation due to refrigerant leakage (Rossi, 2004). An effective fault detection and diagnostic (FDD) system would prevent these losses and reduce the energy usage of the air conditioning equipment.

FDD systems recognize a set of key system performance parameters and function by comparing predicted fault-free parameter values to the current values, and analyzing their residuals. Thus, a reference model is required to estimate the fault-free system parameters at any operating condition. Since a FDD system model requires precise estimation of system parameters, generalized conventional analytical modeling techniques were replaced with empirical correlations in several studies (Gordon and Ng, 1995; Rossi, 1995). Lee et al. (1996) used an artificial neural network to relate the dominant symptoms and faults of an air-handling unit. To improve the modeling capability of a FDD system, Li and Braun (2003) implemented a polynomial/generalized neural network regression in their reference model, and they produced improved interpolation and extrapolation results for a roof top unit. Navarro-Esbri et al. (2007) developed a low-data-requirement model based on neural networks for a water-to-water vapor compression system focused on refrigerant leak detection. In this study we collected extensive data for cooling mode operation of a residential air-source heat pump, and evaluated multivariable polynomial and artificial neural network reference models for their ability to predict system features selected for the FDD scheme.

2. Development of a Fault-Free Steady-State Reference Model

2.1 Tested Heat Pump System

The studied system was a R410A, 8.8 kW (2.5 ton) split residential heat pump with a Seasonal Energy Efficiency Ratio (SEER) of 13 (ARI, 2006). The unit consisted of an indoor fan-coil section, outdoor section with a scroll compressor, cooling mode and heating mode thermostatic expansion valves (TXV), and connecting tubing. Both the indoor and outdoor air-to-refrigerant heat exchangers were of the finned-tube type. The unit was installed in environmental chambers and charged with refrigerant according to the manufacturer's specifications. Figure 1 shows a schematic of the experimental setup indicating the measurement locations of temperature, pressure, and mass flow rate. On the refrigerant side, pressure transducers and T-type thermocouple probes were attached at the inlet and exit of every component of the system. The refrigerant mass flow rate was measured using a Coriolis flow meter. The air enthalpy method served as the primary measurement of the system capacity, and the refrigerant enthalpy method served as the secondary measurement. These two measurements always agreed within 5 %. Table 1 lists uncertainties of the major quantities measured during this work. Detailed specification of the test rig including indoor ductwork, dimensions, data acquisition, measurement uncertainty, and instrumentation was described in Kim et al. (2006).

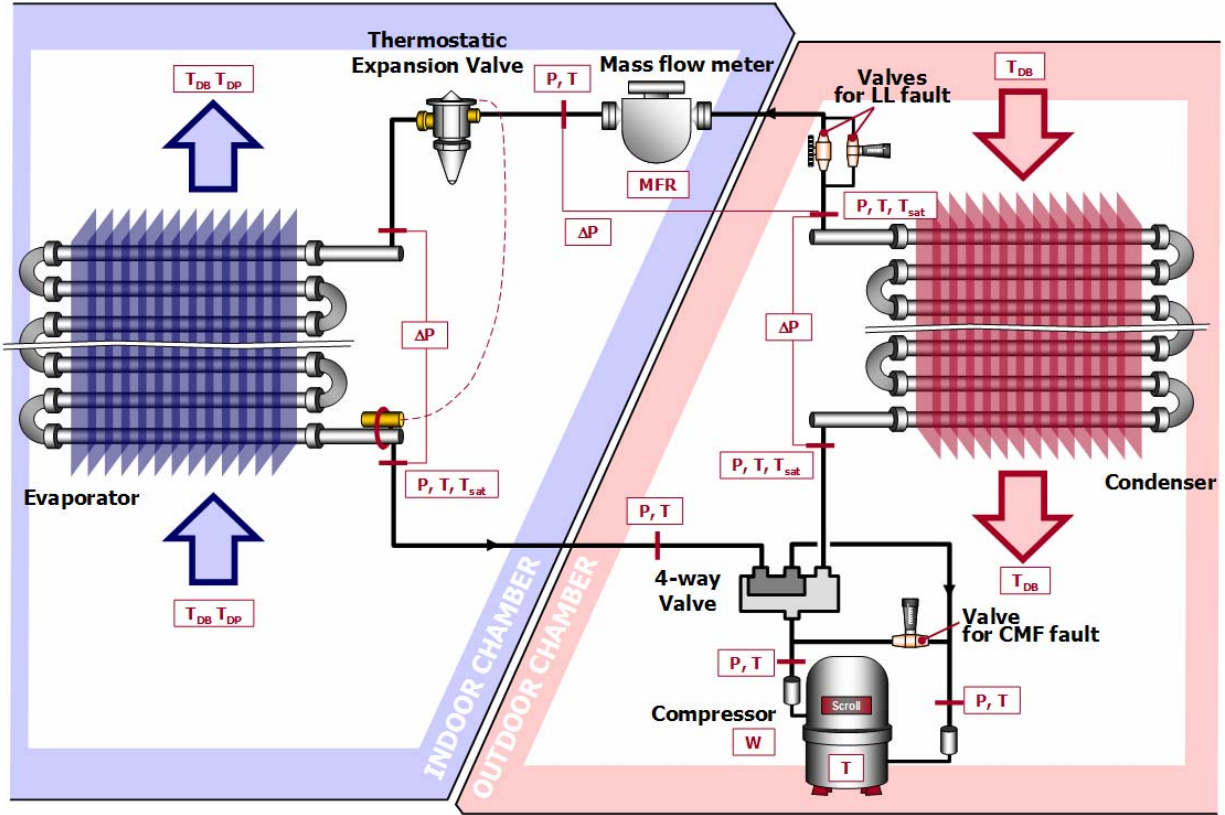


Figure 1. Schematic diagram of the tested heat pump with measurement locations

Table 1. Measurement uncertainties

Measurement	Range	Total Uncertainty at the 95 % Confidence Level
Individual Temperature	-18 °C to 93 °C	±0.3 K
Temperature Difference	0 °C to 28 °C	±0.3 K
Air Nozzle Pressure	0 Pa to 1245 Pa	±1.0 Pa
Refrigerant Mass Flow Rate	0 kg/h to 544 kg/h	±1.0 %
Dewpoint Temperature	-18 °C to 38 °C	±0.4 K
Dry-Bulb Temperature	-18 °C to 40 °C	±0.4 K
Total Cooling Capacity	3 kW to 11 kW	4.0 %
COP	2.5 to 6.0	5.5 %

2.2 Steady-State Detector

The large amount of test data needed to empirically model the cooling mode operation of a heat pump dictated that a consistent and automated method of data acquisition be implemented. For this purpose we used a steady-state detector which determined when the heat pump was in a steady state; thus, the steady-state detector qualified the data that were suitable for inclusion in the dataset used to generate the fault-free steady-state reference models.

The steady-state detector used in our data collection was described in detail by Kim et al. (2007). It focused upon the seven dependent features listed in Table 2. A moving window standard deviation technique was used for monitoring these variables and making a decision as to when steady state occurred. A moving window, as depicted in Figure 2, was characterized by a time (or sample) interval over which

each feature was sampled and saved. The average and standard deviation of the saved data within this time interval were calculated for each feature. The key to using the moving window technique is

Table 2. System features used in fault detection

Independent Features		Dependent Features	
Outdoor dry-bulb temperature	T_{OD}	Evaporator exit refrigerant saturation temperature	T_E
Indoor dry-bulb temperature	T_{ID}	Evaporator exit refrigerant superheat	T_{sh}
Indoor dew point temperature	T_{IDP}	Condenser inlet refrigerant saturation temperature	T_C
		Compressor discharge refrigerant temperature	T_D
		Condenser exit liquid line refrigerant subcooled temperature	T_{sc}
		Evaporator air temperature change	ΔT_{EA}
		Condenser air temperature change	ΔT_{CA}

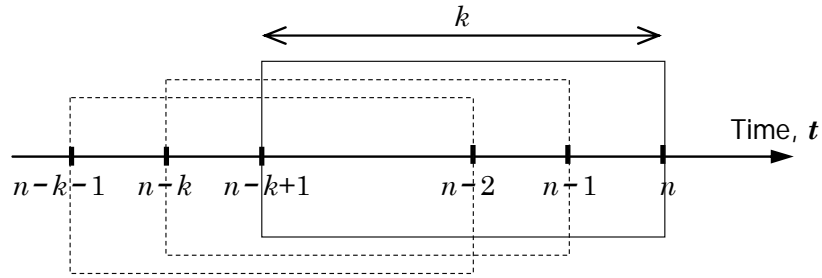


Figure 2. Moving window of k data points at n^{th} time

determining the appropriate moving window size and the standard deviation threshold value for each feature below which the feature is defined to be at steady state.

To illustrate the technique, an example implementation of the steady-state decision is shown in Figure 3(b) where the moving window standard deviation for T_{sh} is shown. As T_{ID} changes, features such as T_{sh} , T_{sc} , and ΔT_{EA} show instability. In this case T_{sh} showed the most fluctuation and was the dominant feature in determining steady state (Figure 3(c)). In most cases, evaporator exit superheat and liquid line subcooling are the two features that determine the steady-state status, but they are not indicative of steady state for all operational conditions; therefore, the steady-state detector monitors all seven features, and all seven features' standard deviations within the moving window must be below their respective threshold values to indicate a steady system. A non steady-state condition for any one feature indicates that the system is not in steady state.

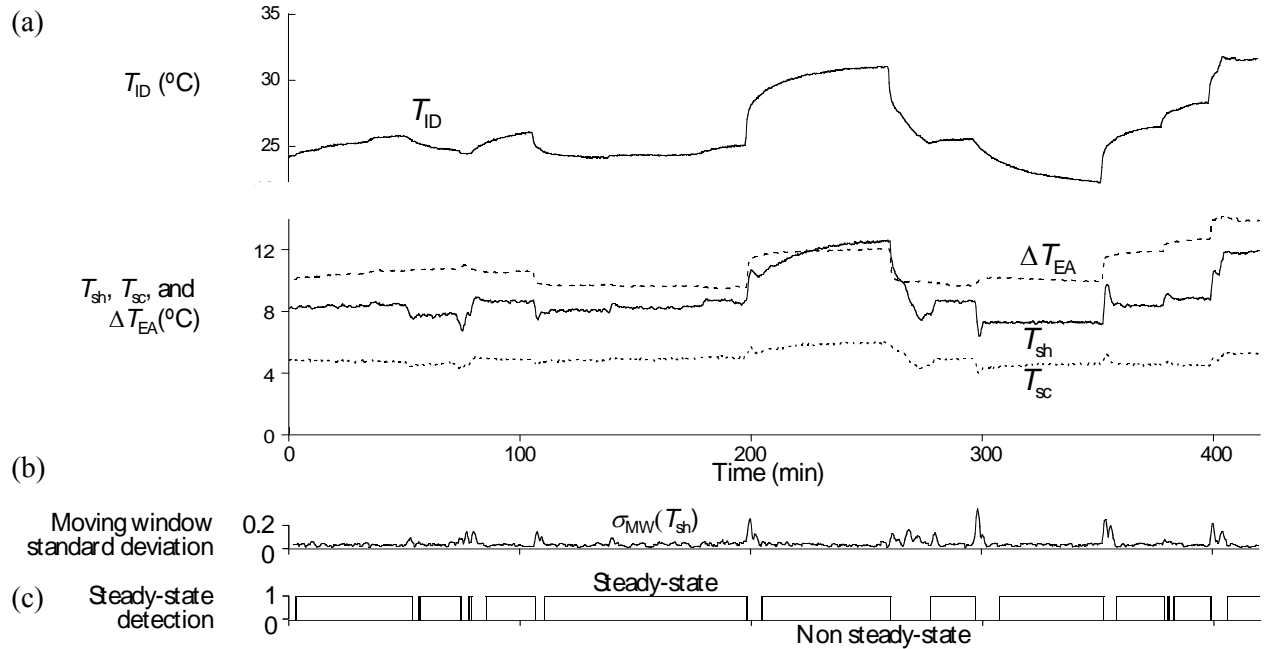


Figure 3. Example of steady-state detection using the moving window standard deviations with T_{sh} being the dominant feature; (a) Measurements of T_{ID} , ΔT_{EA} , T_{sh} , and T_{sc} ; (b) Moving window standard deviation of T_{sh} ; (c) Steady-state status (yes=1, no=0)

2.3 Experimental Method and Conditions

We systematically varied three independent variables, T_{OD} , T_{ID} , and T_{IDP} , and monitored the seven features. To implement the most efficient test procedure, outdoor temperature was fixed at one of four constant values, the addition of steam to the indoor chamber was set at one of several discrete levels by modulating a steam valve, and the indoor dry-bulb temperature was changed over the desired operating range by sequentially energizing ten fixed heaters. For example, as the number of indoor electric heaters increased, the test conditions moved from A to B in Figure 4(a) with indoor temperature increasing. The data were recorded continuously and filtered through the steady-state detector, which qualified steady-state data for use in development of the reference model. In this process, instability of the system due to on-off transients and rapid load changes was filtered out by the steady-state detector.

Table 3 shows operating conditions for the fault-free tests. The four outdoor temperatures were maintained within ± 0.3 °C. For the indoor conditions, the amount of steam introduced to the indoor chamber was fixed such that the humidity ratio varied from 0.0037 to 0.0168. Data were recorded, every 18 s, as indoor dry-bulb temperature varied from 15.3 °C to 33.9 °C. The range of operating conditions for which data were collected defines the applicable limits for the FDD scheme.

Table 3. Operating conditions for fault-free tests

Outdoor DB temp. (°C)	27.8, 32.2, 35.0, 37.8
Indoor DB temp. (°C)	15.3 to 33.9
Indoor humidity ratio	0.0037 to 0.0168

From the total number of 10409 recorded data sets, 5830 data sets passed through the steady-state detector. Among these steady-state sets, 2176 sets were collected at 27.8 °C outdoor temperature, 1732 sets at 32.2 °C, 633 sets at 35.0 °C, and 1289 sets at 37.8 °C. Figure 4(b) shows a sample of data (every fifth data point) taken at four fixed outdoor temperatures. In addition, we performed ARI standard rating

tests at 27.8 °C indoor and 35.0 °C outdoor dry-bulb temperatures (ARI, 2006) and included these data to develop the fault-free steady-state reference models.

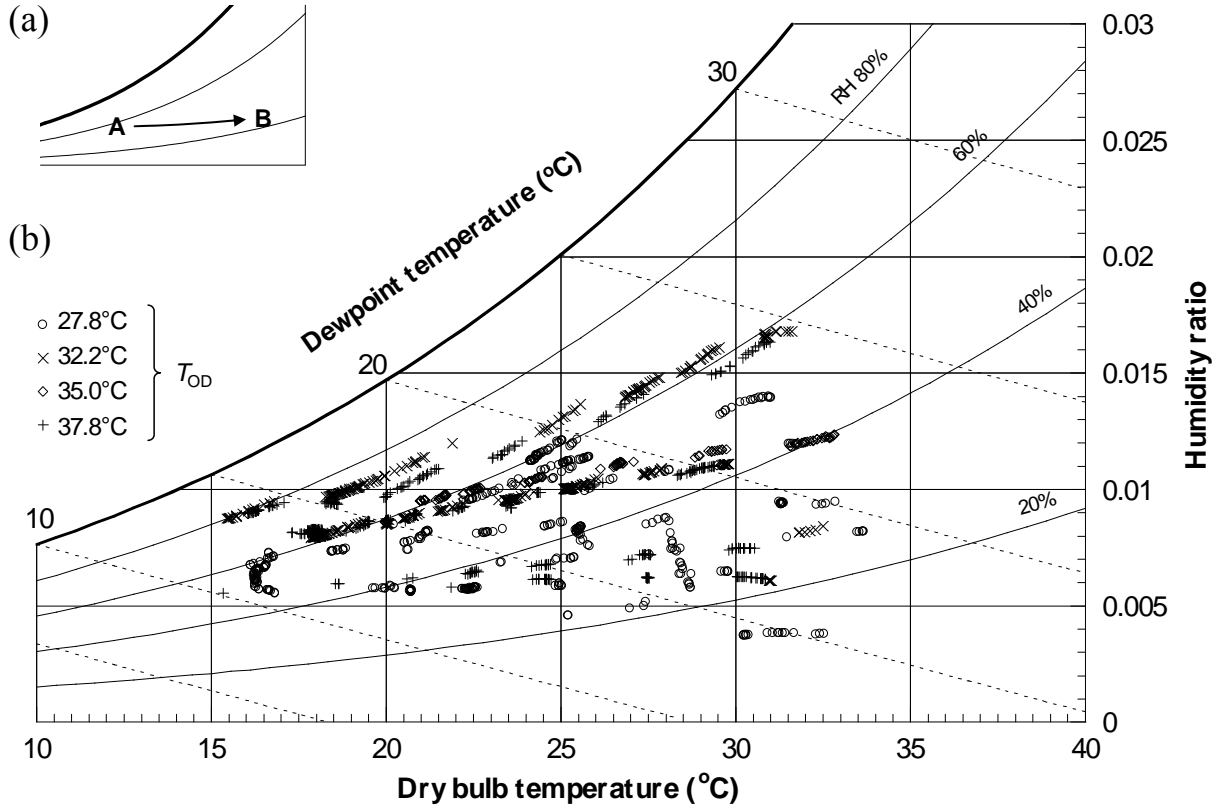


Figure 4. Indoor test conditions on a psychrometric chart for fault-free model experiments at a fixed outdoor temperature; (a) Indoor condition change as electric heaters activate; (b) Sampled indoor air conditions at T_{OD} of 27.8, 32.2, 35.0, and 37.8

2.4 Multivariable Polynomial Regression (MPR) Reference Model

The MPR model belongs to the “black-box” category of models, which do not consider the physics of the system and require a large data set to accurately predict a system’s performance. In our study, we evaluated 1st, 2nd, 3rd, and 4th order MPR models representing the seven key features of the heat pump. The higher order MPR models offer better accuracy of prediction; however, excessive polynomial order for a relatively small database may worsen data interpolation. The MPR models presented in this work have an advantage in that they have a simple structure and can be programmed easily. In addition, they can be implemented for any other experimental database with little modification, because they have no physical basis.

We used outdoor dry-bulb temperature (T_{OD}), indoor dry-bulb temperature (T_{ID}), and indoor dew point temperature (T_{IDP}) as independent variables. These variables were regressed upon the database generated from the fault-free tests. Equations (1a), (1b), (1c), and (1d) show the general form of the regressed equations for the i^{th} feature (or i^{th} dependent variable) as 1st, 2nd, 3rd, and 4th order MPR models, respectively.

$$\phi_i^{(1)} = a_0 + a_1 T_{OD} + a_2 T_{ID} + a_3 T_{IDP} \quad (1^{\text{st}} \text{ order}) \quad (1a)$$

$$\phi_i^{(2)} = \phi_i^{(1)} + a_4 T_{OD}^2 + a_5 T_{ID}^2 + a_6 T_{IDP}^2 + a_7 T_{OD} T_{ID} + a_8 T_{ID} T_{IDP} + a_9 T_{IDP} T_{OD} \quad (2^{\text{nd}} \text{ order}) \quad (1b)$$

$$\begin{aligned} \phi_i^{(3)} = & \phi_i^{(2)} + a_{10}T_{OD}^3 + a_{11}T_{ID}^3 + a_{12}T_{IDP}^3 + a_{13}T_{OD}T_{ID}T_{IDP} \\ & + a_{14}T_{OD}^2T_{ID} + a_{15}T_{OD}^2T_{IDP} + a_{16}T_{ID}^2T_{OD} + a_{17}T_{ID}^2T_{IDP} + a_{18}T_{IDP}^2T_{OD} + a_{19}T_{IDP}^2T_{ID} \end{aligned} \quad (3^{rd} \text{ order}) \quad (1c)$$

$$\begin{aligned} \phi_i^{(4)} = & \phi_i^{(3)} + a_{20}T_{OD}^4 + a_{21}T_{ID}^4 + a_{22}T_{IDP}^4 + a_{23}T_{ID}^2T_{OD}^2 + a_{24}T_{ID}^2T_{IDP}^2 + a_{25}T_{IDP}^2T_{OD}^2 \\ & + a_{26}T_{ID}T_{OD}^3 + a_{27}T_{ID}T_{IDP}^3 + a_{28}T_{IDP}T_{OD}^3 + a_{29}T_{ID}^3T_{OD} + a_{30}T_{ID}^3T_{IDP} + a_{31}T_{IDP}^3T_{OD} \\ & + a_{32}T_{ID}^2T_{OD}T_{IDP} + a_{33}T_{ID}T_{OD}^2T_{IDP} + a_{34}T_{ID}T_{OD}T_{IDP}^2 \end{aligned} \quad (4^{th} \text{ order}) \quad (1d)$$

2.5 Artificial Neural Network (ANN) Reference Model

An Artificial Neural Network (ANN) model was developed for the seven features. The relationship of independent variables and features is learned by an artificial neural network using a back propagation algorithm (Wasserman, 1989; Hassoun, 1995). Figure 5 shows the structure of the ANN used in this study. It has three input variables (T_{OD} , T_{ID} , and T_{IDP}) and one output. This neural network has three layers consisting of an input, hidden, and output layer with the input and hidden layers having three nodes. The sigmoid function is used as the activation function of the hidden layer. The weight coefficients and offsets are “learned” using a momentum back propagation algorithm through more than 10,000 iterations.

The input layer acts only as input nodes; no processing of T_{OD} , T_{ID} , or T_{IDP} occurs within the input layer. The various arrows between the input layer and the hidden layer indicate weights, or multipliers, applied to each input variable before passing to the sigmoid function within each hidden layer node. Equation 2 illustrates the output of a neuron, $f(s)$, and how the sigmoid function is applied within the layers.

$$f(s) = \frac{1}{2}(1 + \tanh(2s)) \quad s = \left(\sum_{k=1}^3 x_k w_k \right) + c \quad (2)$$

The three-node hidden layer uses 9 adjustable weighting coefficients and 3 offset coefficients. The single output node has its own 3 adjustable weighting coefficients and a single offset to produce the final predicted value of the feature, F_{pred} . Each heat pump feature to be represented by the ANN is calculated in this manner using T_{OD} , T_{ID} , or T_{IDP} as inputs. The predicted value is compared to the measured value to produce an error value (residual) for each feature. The back propagation algorithm is then used to adjust the weights and offsets to minimize the error, or “train” the ANN.

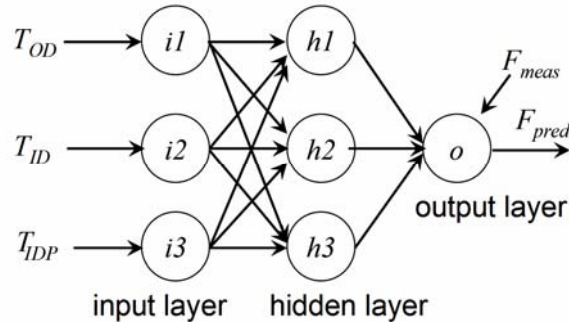


Figure 5. Artificial neural network structure

3. Model Validation

In validating the model, we used a dataset of 111 points, a subset of the full 5830 point dataset, to improve the performance of the ANN learning process. The 111 point dataset was created by selecting the datapoints that were spaced by a minimum predetermined distance in the independent variables space. First, T_{ID} , T_{OD} , and T_{IDP} were mapped onto xyz -coordinates. Each (x, y, z) point was then compared to

all of the other points to determine if any of the other points fell within the predetermined distance of the point. This is equivalent to drawing a sphere of radius r at a particular (x, y, z) location and examining this sphere volume to determine if any other points fall within. If another (x, y, z) point fell within this sphere, it was removed from the data set; thus all of the independent variable (x, y, z) points were examined and winnowed in this manner. In this study, r was selected to be $0.96\text{ }^\circ\text{C}$.

Table 4 shows the mean squared residual (MSR), as calculated by Eq. 3, for the multivariate polynomial regression models and ANN model when fit to the reduced dataset consisting of 111 points. The mean squared residual is the sum of the squared residuals divided by the degrees of freedom for the regression and is an estimate of the model variance (Graybill and Iyer, 1994a).

$$\text{MSR} = \frac{\sum_i (x_i - \phi_i^{(n)})^2}{N - (m + 1)} \quad (3)$$

Table 4. MSR of the models fit to a reduced dataset of 111 points for the seven selected features

Feature	1 st order	2 nd order	3 rd order	4 th order	ANN
T_E ($^\circ\text{C}$)	1.298	0.095	0.052	0.016	0.122
T_{sh} ($^\circ\text{C}$)	0.980	0.442	0.222	0.140	0.263
T_C ($^\circ\text{C}$)	0.136	0.014	0.007	0.005	0.072
T_D ($^\circ\text{C}$)	2.215	0.373	0.246	0.110	1.341
T_{sc} ($^\circ\text{C}$)	0.198	0.139	0.081	0.036	0.395
ΔT_{EA} ($^\circ\text{C}$)	1.431	0.087	0.030	0.012	0.159
ΔT_{CA} ($^\circ\text{C}$)	0.106	0.019	0.012	0.009	0.024
m+1	4	10	20	35	16

Table 5 shows the MSRs for the models fit to the full dataset of 5830 points while Table 6 shows the MSRs for the reduced dataset models applied to the full dataset. The reduced models' MSRs of Table 6 and the full dataset MSRs of Table 5 differ by an average of 26 %. Thus the reduced dataset is a good representation of the system features, but the full dataset model produces smaller MSRs.

Table 5. MSR of the models fit to the full dataset of 5830 points for the seven selected features

Feature	1 st order	2 nd order	3 rd order	4 th order	ANN
T_E ($^\circ\text{C}$)	0.979	0.072	0.051	0.015	0.129
T_{sh} ($^\circ\text{C}$)	1.055	0.397	0.176	0.121	0.273
T_C ($^\circ\text{C}$)	0.108	0.011	0.007	0.005	0.068
T_D ($^\circ\text{C}$)	2.078	0.342	0.213	0.088	1.403
T_{sc} ($^\circ\text{C}$)	0.202	0.135	0.066	0.028	0.480
ΔT_{EA} ($^\circ\text{C}$)	1.103	0.066	0.027	0.011	0.159
ΔT_{CA} ($^\circ\text{C}$)	0.085	0.018	0.014	0.012	0.030
m+1	4	10	20	35	16

Table 6. MSR of the reduced dataset model applied to the full dataset of 5830 points for the seven selected features

Feature	1 st order	2 nd order	3 rd order	4 th order	ANN
T_E ($^\circ\text{C}$)	0.992	0.077	0.061	0.023	0.129
T_{sh} ($^\circ\text{C}$)	1.160	0.465	0.258	0.213	0.273

T_C (°C)	0.110	0.012	0.0080	0.0078	0.068
T_D (°C)	2.403	0.409	0.285	0.161	1.407
T_{sc} (°C)	0.213	0.144	0.083	0.055	0.482
ΔT_{EA} (°C)	1.116	0.072	0.033	0.017	0.160
ΔT_{CA} (°C)	0.087	0.019	0.017	0.019	0.030
m+1	4	10	20	35	16

As expected, a higher order MPR model produces a smaller mean squared residual. However, the number of model coefficients increases exponentially due to the addition of the crossterm coefficients. The number of coefficients, m+1, used to model each feature may be reduced by applying an F-Test to each coefficient of the respective models (Graybill and Iyer, 1994b). The F-statistic is calculated using the following equations:

$$MS_{\text{drop}} = \frac{(\text{SSR}_{\text{reduced}} - \text{SSR}_{\text{full}})}{m - g} \quad (4)$$

$$\text{MSR}_{\text{full}} = \frac{\text{SSR}_{\text{full}}}{N - (m + 1)} \quad (5)$$

$$F = \frac{MS_{\text{drop}}}{\text{MSR}_{\text{full}}} \quad (6)$$

where g+1 is the number of coefficients in the reduced model. The F-statistic follows an F distribution with m-g and N-(m+1) degrees of freedom. Large values of F indicate that the terms removed from the reduced model were significant. One may use the F-statistic as a means of ranking the contribution of a particular coefficient to the fit of the regressed model. By dropping one term at a time and sorting the reduced models in terms of their F-statistics, the effect of removal of a particular term may be assessed by comparing the MSR of the reduced model to that of the full model. Table 7 shows the results of this technique when applied to a backward elimination on the full 3rd order polynomial model.

Table 7. Terms removed from the 3rd order MPR model using an F-Test

3 rd Order MPR Model Backward Elimination, $x = T_{OD}$, $y = T_{ID}$, $z = T_{IDP}$			
Feature	Less than 1 % higher MSR	Less than 5 % higher MSR	Less than 10 % higher MSR
Term(s) removed			
T_E (°C)	z, xy, z^2	z, xy, z^2, x^2, y, y^3	NA
T_{sh} (°C)	y^2, z, z^2, y^2z, x	$y^2, z, z^2, y^2z, x, y, z^3$	$y^2, z, z^2, y^2z, x, y, z^3, y^2x,$ y^3
T_C (°C)	y	y, y^2z, y^3	y, y^2z, y^3, yz, z^3
T_D (°C)	x, y^3	$x, y^3, yz, x^2y, z^2y, xyz$	$x, y^3, yz, x^2y, z^2y, xyz, z^2$
T_{sc} (°C)	y, z^2, z^2y, y^3	$y, z^2, z^2y, y^3, y^2x, yz, z^2x$	NA
ΔT_{EA} (°C)	y	NA	y, z
ΔT_{CA} (°C)	x^2z, y, z^3	$x^2z, y, z^3, y^3, z, x^2y, xz$	NA

NA: The % change in MSR does not fall between the upper and lower bounds with the removal of a single coefficient.

Table 7 shows that one to four terms may be removed from the full 3rd order polynomial while the models' MSR's remain less than 1 % from the full models' MSR's. If the criteria is raised to within 5 % of

the full models' MSR, up to seven terms may be removed from several of the 3rd order polynomials. Raising the percentage change in MSR to within 10 % allows the removal of up to nine coefficients for T_{sh} . The decision as to how many terms to remove is at the discretion of the model developer, but as with any regression equation, the confidence interval on the mean value of any of the features determined at a particular value of the independent parameters will be larger for larger MSRs. The confidence interval is a function of the MPR model standard residual (\sqrt{MSR}), the Student's t-value for the particular confidence level, and degrees of freedom (Ott 1984).

Figure 6 shows the performance of the full MPR models and ANN model during operation at a T_{OD} of 27.8 ± 0.3 °C. If an air conditioning system is installed in the field, T_{ID} may change continuously according to indoor cooling load or thermostat settings. The three features, T_{sh} , T_{sc} , and T_D , are shown in Figure 6 because they varied the most as indoor temperature changed. In Figure 6(a) where there is an abrupt change in T_{ID} , the steady state of the system is broken, as indicated by the steady-state detector in Figure 6(e).

Figure 6(b), 6(c), and 6(d) show T_{sh} , T_{sc} and T_D as predicted by the 1st, 2nd, and 3rd order MPR models and the ANN model. The 3rd order MPR model shows the best fit to the measured data during steady-state operation. As the order of the polynomial model decreases, the fit to the experimental data set degrades. Predictions by the ANN model are worse than those by the 3rd order MPR model. The T_{sh} predicted by the ANN model is comparable to that of the 3rd order MPR model (Figure 6(b)), but T_{sc} was not predicted well by the ANN model, as shown in Figure 6(c). The predicted values of T_D for the ANN model are between the 1st and 2nd order MPR models, as shown in Figure 6(d).

4. Summary

Seven features of a residential heat pump system were modeled using the 1st, 2nd, 3rd, and 4th order MPR models and an ANN model. The laboratory data were filtered by a steady-state detector, which automatically examined and processed data to improve data collection consistency and the resulting steady-state reference model. Considering the fit, the polynomial model should be at least 3rd order. The 4th order polynomial model's use of 75 % more coefficients for only a 14 % decrease in MSR does not justify it replacing the 3rd order model. The F-Test can be applied to reduce the number of coefficients in a general linear model, and this technique may aid a developer in creating a more compact representation of the system features. The ANN model predicted all features with less accuracy than the 3rd order MPR model. Because of insignificant non-linearity between the independent variables and the features in the cooling mode, the ANN model's ability to fit nonlinear behavior did not provide any advantage over the 3rd order MPR models.

The reference model should not be over-specified by increasing the order of the MPR model. The model variance should be lower than that of independent variable measurements. The smaller the models' variances, the smaller their contribution to the overall uncertainty of the predicted features. The model developer must decide on an acceptable level of model variance based upon his FDD requirements and his ability to measure the independent variables and features.

Acknowledgment

Seok Ho Yoon's research at the National Institute of Standards and Technology, Gaithersburg, MD, was supported by a Korea Research Foundation Grant funded by the Korean Government (MOEHRD, KRF-2005-214-D00240).

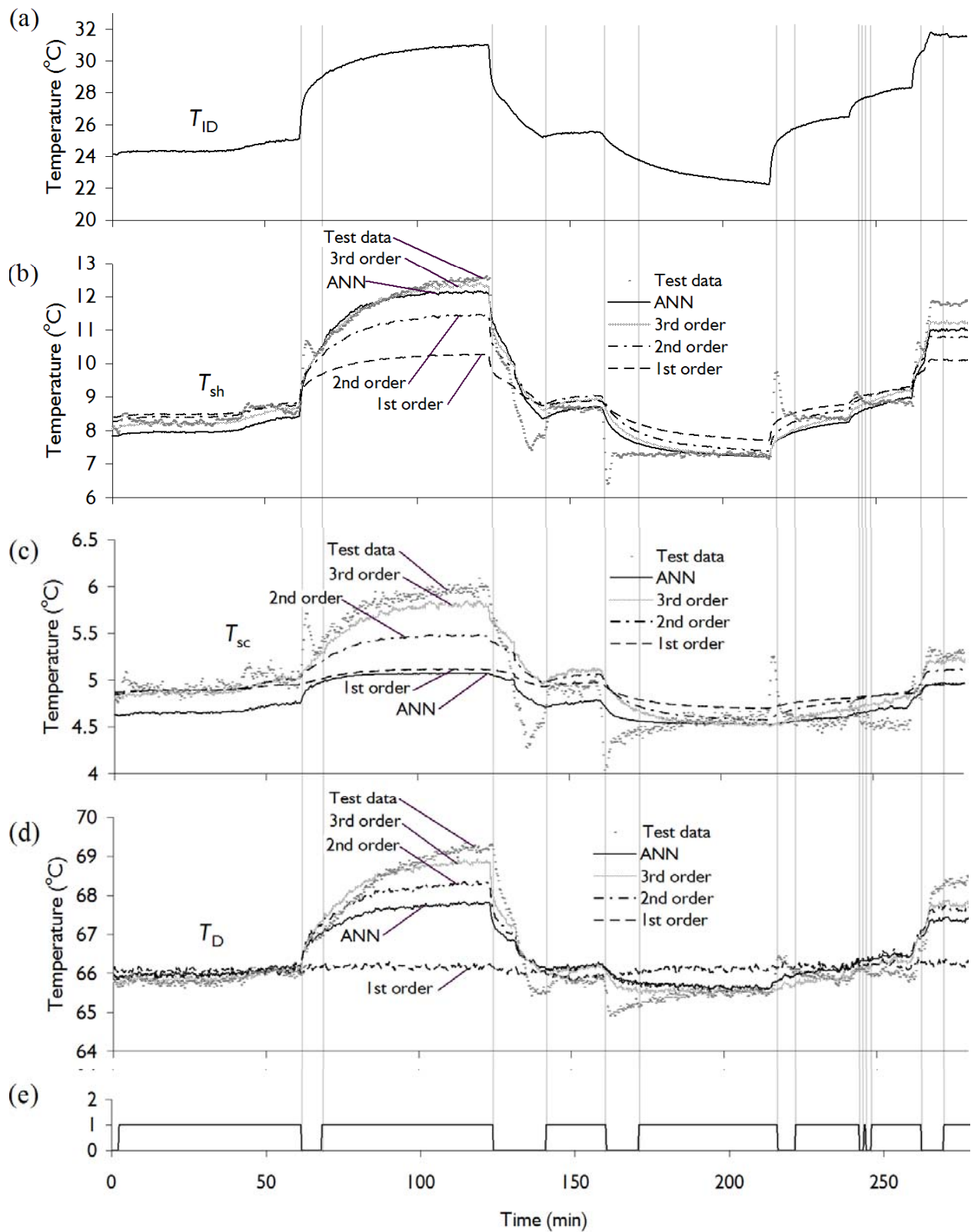


Figure 6. Performance of MPR models and ANN model to predict features during a sample operation period; (a) T_{ID} ; (b) T_{sh} ; (c) T_{sc} ; (d) T_D ; (e) Steady-state status (yes =1, no = 0)

References

- ARI, 2006, "Performance rating of unitary air conditioning and air source heat pump equipment," ARI Standard 210/240, Air Conditioning and Refrigeration Institute, Arlington, VA, USA
- Gordon, J. M. and Ng, K. C., 1995, "Predictive and diagnostic aspects of a universal thermodynamic model for chillers," *International Journal of Heat and Mass Transfer*, Vol. 38, No. 5, pp. 807-818.
- Graybill, F. A. and Iyer, H. K., 1994a, *Regression analysis: concepts and applications*, 2nd edition, Duxbury Press, Belmont California, pp. 239-241.
- Graybill, F. A. and Iyer, H. K., 1994b, *Regression analysis: concepts and applications*, 2nd edition, Duxbury Press, Belmont California, pp. 431-437.
- Hassoun, M.H., 1995, "Fundamentals of Artificial Neural Networks", The MIT Press, Cambridge, MA.
- Kim, M., Payne, W. V., Domanski, P. A., and Hermes, C. J. L., 2006, "Performance of a residential heat pump operating in the cooling mode with single faults," NISTIR 7350, National Institute of Standards and Technology, Gaithersburg, MD, USA.
- Kim, M., Yoon, S. H., Payne, W. V., and Domanski, P. A., 2007, "Design of a steady-state detector for fault detection and diagnosis of a residential air conditioner," Accepted for publication by the *International Journal of Refrigeration*, [doi:10.1016/j.ijrefrig.2007.11.008](https://doi.org/10.1016/j.ijrefrig.2007.11.008) .
- Lee, W.-Y., House, J.M., Park, C., and Kelly, G.E., 1996, "Fault Diagnosis of an Air-Handling Unit Using Artificial Neural Networks", *ASHRAE Transactions*, Vol. 102, Pt. 1, pp. 540-549.
- Li, H. and Braun, J.E., 2003, "An Improved Method for Fault Detection and Diagnosis Applied to Package Air Conditioners," *ASHRAE Transactions*, Vol. 109, Part 2, pp. 683-692.
- Navarro-Esbri J., Torrella E, Cabello R., 2007, "A vapour compression chiller fault detection technique based on adaptive algorithms. Application to on-line refrigerant leakage detection," *International Journal of Refrigeration*, Vol. 29, pp. 716-723.
- Ott, L., 1984, *An introduction to statistical methods and data analysis*, 2nd edition, PWS Publishers, Duxbury Press, Boston, Massachusetts, ISBN 0-87150-473-1, pp. 438-443.
- Proctor, J., 2004, "Residential and Small Commercial Central Air Conditioning; Rated Efficiency isn't Automatic," Presentation at the Public Session. ASHRAE Winter Meeting, January 26, Anaheim, CA.
- Rossi, T.M., 1995, *Detection, diagnosis, and evaluation of faults in vapor compression cycle equipment*, Ph.D. Thesis, Purdue University, West Lafayette, IN, USA
- Rossi, T.M., 2004, "Unitary Air Conditioner Field Performance," *International Refrigeration and Air Conditioning Conference at Purdue*, Paper No. R146, July 12-15, West Lafayette, IN.
- Wasserman, P.D., 1989, "Neural Computing Theory and Practice", Van Nostrand Reinhold, New York, NY.

List of Tables

- Table 1. Measurement uncertainties
Table 2. System features used in fault detection
Table 3. Operating conditions for fault-free tests
Table 4. MSR of the models fit to a reduced dataset of 111 points for the seven selected features
Table 5. MSR of the models fit to the full dataset of 5830 points for the seven selected features
Table 6. MSR of the reduced dataset model applied to the full dataset of 5830 points for the seven selected features
Table 7. Terms removed from the 3rd order MPR model using an F-Test

List of Figures

- Figure 1. Schematic diagram of the tested heat pump with measurement locations
Figure 2. Moving window of k data points at n^{th} time
Figure 3. Example of steady-state detection using the moving window standard deviations with T_{sh} being the dominant feature; (a) Measurements of T_{ID} , ΔT_{EA} , T_{sh} , and T_{sc} ; (b) Moving window standard deviation of T_{sh} ; (c) Steady-state status (yes=1, no=0)
Figure 4. Indoor test conditions on a psychrometric chart for fault-free model experiments at a fixed outdoor temperature; (a) Indoor condition change as electric heaters activate; (b) Sampled indoor air conditions at T_{OD} of 27.8, 32.2, 35.0, and 37.8
Figure 5. Artificial neural network structure
Figure 6. Performance of MPR models and ANN model to predict features during a sample operation period; (a) T_{ID} ; (b) T_{sh} ; (c) T_{sc} ; (d) T_{D} ; (e) Steady-state status (yes =1, no = 0)